Nanoscale Res Lett (2009) 4:820–827
DOI 10.1007/s11671-009-9321-y

NANO EXPRESS

Crystalline Gaq_3 Nanostructures: Preparation, Thermal Property and Spectroscopy Characterization

Ya-Wen Yu · Chun-Pei Cho · Tsong-Pyng Perng

Received: 25 February 2009 / Accepted: 8 April 2009 / Published online: 30 April 2009

Abstract Crystalline Gaq_3 1-D nanostructures and nanospheres could be fabricated by thermal evaporation under cold trap. The influences of the key process parameters on formation of the nanostructures were also investigated. It has been demonstrated that the morphology and dimension of the nanostructures were mainly controlled by working temperature and working pressure. One-dimensional nanostructures were fabricated at a lower working temperature, whereas nanospheres were formed at a higher working temperature. Larger nanospheres could be obtained when a higher working pressure was applied. The XRD, FTIR, and NMR analyses evidenced that the nanostructures mainly consisted of δ-phase Gaq_3. Their DSC trace revealed two small exothermic peaks in addition to the melting endotherm. The one in lower temperature region was ascribed to a transition from δ to β phase, while another in higher temperature region could be identified as a transition from β to δ phase. All the crystalline nanostructures show similar PL spectra due to absence of quantum confinement effect. They also exhibited a spectral blue shift because of a looser interligand spacing and reduced orbital overlap in their δ-phase molecular structures.

Y.-W. Yu · T.-P. Perng
Department of Materials Science and Engineering, National Tsing Hua University, Hsinchu 30013, Taiwan

C.-P. Cho
Department of Applied Materials and Optoelectronic Engineering, National Chi Nan University, Nantou 54561, Taiwan
e-mail: emily.cho31@msa.hinet.net

T.-P. Perng (✉)
Department of Chemical Engineering and Materials Science, Yuan Ze University, Chung-Li 32003, Taiwan
e-mail: tpperng@mx.nthu.edu.tw

Keywords Gaq_3 · 1-D nanostructures · Nanospheres · Thermal evaporation · Crystallization · Phase transition

Introduction

In the last decade, nanoscale materials have drawn considerable attention because they present an extremely high surface area to volume ratio which makes a certain number of optical, electrical, mechanical, and physical properties apparently different from those of their counterpart bulk solids [1–3]. Among the nanoscale materials, one-dimensional (1D) form is particularly attractive because it may provide access to three different contact regions, inner and outer surfaces as well as both ends. One-dimensional nanomaterials can also be used as the building blocks for nanoscale devices. A number of studies have been devoted to generate 1-D nanomaterials from most kinds of materials, which clearly indicate that solid materials can be prepared as 1-D nanostructures by properly selected preparation methods [4]. However, the efforts were mostly focused on inorganic or metallic nanomaterials. Only few studies concerning organic nanomaterials have been reported [5–8]. Until recently, it has been demonstrated that some 1-D organic nanostructures exhibit promising applications for optoelectronic devices due to their unique characteristics such as flexibility, high photoconductivity, nonlinear optical effects, good field-effect mobilities, and remarkable chemical and thermal stabilities [9–11]. Therefore, more exploration of 1-D organic nanostructures is certainly required, and precise morphological control of the organic nanostructures has to be obtained before practical applications. Previously it has been reported that single-crystalline copper phthalocyanine (CuPc) nanoribbons with a good controlled

diameter ranging from 50 to 125 nm could be formed by physical vapor transport technique. Various architectures of organic field-effect transistors (OFETs) based on patterned CuPc nanoribbons were also achieved [12–14].

8-Hydroxyquinoline metal chelate complexes (Mq_3), one type of the organic semiconducting materials, are attracting increasing interests because they can be employed in organic light-emitting diodes (OLEDs) as an electron transport and emitting material [15–17]. They not only contribute to lower operational voltages and high efficiency of the devices, but also provide the capability for color tuning which can be achieved by grafting different substituents [16]. Among the Mq_3, tris(8-hydroxyquinolinato)aluminium(III) (Alq_3) is most well known and has been frequently used in OLEDs due to its stability and good charge transport ability. Its fundamental characteristics, such as molecular geometry and molecular orbitals, have also been explicitly reported [18, 19]. More recently, it was demonstrated that Alq_3 nanostructures could be prepared by means of physical thermal evaporation [20–23]. The amorphous Alq_3 nanoparticles could grow into α-phase crystalline nanowires by a one-step heat treatment process. A complete structural transformation to crystalline nanowires would lead to a blue shift and enhanced intensity of the photoluminescence (PL) spectrum [20, 21]. Some inorganic semiconductor quantum dots also exhibited outstanding optical properties due to the large oscillator strengths, narrow spectral linewidths, and high stability, so that they could be easily integrated inside devices [24, 25]. Unfortunately, the rigidity and bio-uncompatibility of most inorganic nanomaterials will be bottlenecks limiting their applications to flexible and biological devices. Thus for long-term development tendency, organic semiconductor nanostructures reveal more potential and advantages, as compared to inorganic nanomaterials.

Tris(8-hydroxyquinoline)gallium(III) (Gaq_3), another Mq_3 first reported by Burrows et al., could provide a higher electroluminescence yield than Alq_3 when it was used in OLEDs. This suggested that it could be a more promising candidate as an electron transport and emitting material. [26–28]. Therefore, the preparation method, optical, physical, and crystallographic characteristics of Gaq_3 nanostructures are worthy of further investigation. In this work, a similar thermal evaporation approach for fabrication of Gaq_3 nanowires and nanospheres was disclosed. The key process parameters such as working gas, working temperature, and working pressure were varied to achieve various morphologies and dimensions. It was demonstrated that the nanostructures mainly consisted of δ-phase Gaq_3. The DSC analysis of crystalline nanospheres revealed a transition from δ to β phase in the lower temperature region and another transition from β to δ phase in the higher temperature region. All the nanostructures showed similar PL spectra and a spectral blue shift due to a looser interligand spacing and reduced orbital overlap in the crystalline nanostructures.

Experimental

Gaq_3 nanowires and nanospheres could be fabricated by thermal evaporation. The schematic thermal evaporation system had been presented elsewhere [29]. This system mainly consists of four parts: a process chamber, a pumping system, a gauge system, and a heating system. Two graphite electrodes are installed in the middle of the process chamber. A graphite boat spanning across the two electrodes is used as a resistive heater. The DC current applied to the graphite boat is converted by a power supply transformer. A K-type thermocouple in contact with the boat is employed to control the working temperature. The conjunctional circuits of the power supply, thermocouple, and cooling water are arranged below outside the process chamber. A movable shutter is utilized to control evaporation time. The pumping system including a rotary vane pump and a turbo pump is able to evacuate the process chamber down to a pressure lower than 1×10^{-6} torr. The top of the process chamber is a liftable cap with a hollow cavity inside. Liquid nitrogen can be poured into and fill the cavity for rapid uniform cooling of the *n*-type (100) silicon substrates. The substrates were repeatedly ultrasonically rinsed in acetone followed by dry purge of N_2 gas before use. They were then adhered to the underside of the cap for growth of Gaq_3 nanostructures. A stainless steel ring was put on the graphite boat, and commercial Gaq_3 powder was placed into the ring. The distance between the graphite boat and the substrate was fixed at 10 cm.

The working gases used in this study are He and Ar. After the process chamber was evacuated to 1×10^{-6} torr, the working gas was introduced into the chamber. Once the graphite boat was heated to the working temperature, the shutter was moved away and thermal evaporation started. Meanwhile, liquid nitrogen was poured into the hollow cavity for cold trap of sublimed Gaq_3 molecules on the substrate. After the condensation was complete, the process chamber was evacuated again, and the whole system returned to room temperature. The key process parameters in the thermal evaporation process are working gas, working pressure, and working temperature, etc. Various parameters cause dissimilar nanostructures. The working pressures of 10 and 50 torr and the working temperatures ranging from 310 to 400 °C were adopted to investigate their influences on the morphology and dimension of nanostructures by a field emission scanning electron microscope (FESEM, JEOL-JSM6500F). An X-ray diffraction (XRD) spectrometer (Shimazu-Mode-XRD-6000)

with Cu Kα radiation ($\lambda = 1.545$Å) and a scanning rate of 1 deg/min was employed to examine the crystallinity of Gaq_3 powder and nanostructures. A differential scanning calorimeter (DSC, Seiko 220C) with a heating rate of 20 °C/min was used to analyze their thermal properties. The infrared (IR) spectra were achieved by a fourier transform infrared (FTIR) spectrometer (HORIBA FT-730) with a scanning rate of 5 mm/s and a resolution of 4 cm^{-1} to identify their isomorphism. The nuclear magnetic resonance (NMR) spectra were obtained by the spectrometers of Bruker DSX400WB and Varian Unityinova 500. Their PL spectra ranging from 400 to 700 nm were measured using a fluorescence spectrometer (Perkin Elmer LS55) with an excitation wavelength of 390 nm and a scanning rate of 500 nm/min.

Results and Discussion

(1) Preparation of Gaq_3 nanostructures

The key parameters of the thermal evaporation process such as working gas, working temperature, and working pressure were altered in order to achieve various Gaq_3 nanostructures. When the working gas is He and the working temperature is lower than 350 °C, 1-D Gaq_3 nanostructures with a diameter ranging from 40 to 80 nm and a length of 100–600 nm are formed, as shown in Fig. 1. No matter the working temperature is 310 or 330 °C in He, longer nanowires can be obtained at a lower working pressure (10 torr), and shorter 1-D nanostructures are acquired at a higher working pressure (50 torr). It is perceived that the working pressure of He is certainty crucial to the length but shows no apparent influence on the diameter of the 1-D nanostructures. When the working temperature increased to 350 °C, similar Gaq_3 1D nanostructures were also observed under various working pressures of He. They accompanied with few aggregations of small nanoparticles especially at a higher working pressure (not shown). As the working temperature raises to 370 °C, a network of connected small Gaq_3 nanoparticles are fabricated at a lower working pressure (10 torr), whereas 1-D nanostructures along with some larger merged nanoparticles are observed at a higher working pressure (50 torr), as shown in Fig. 2. When the working temperature is further raised to 390 or 400 °C, only nanospheres with a smooth surface are observed, as displayed in Fig. 3. Their size is larger than the nanoparticles obtained at a lower working temperature (370 °C). Smaller nanospheres are formed at 10 torr of He no matter the working temperature is 390 or 400 °C, as revealed in Fig. 3a and c. Larger nanospheres can be observed at a higher working pressure of He (50 torr), as shown in Fig. 3b and d. Their diameter ranges from 200 to 400 nm as the working temperature is 390 °C (Fig. 3b). A wider distribution range of diameter from 300 to 700 nm is demonstrated when the working temperature increases to 400 °C (Fig. 3d).

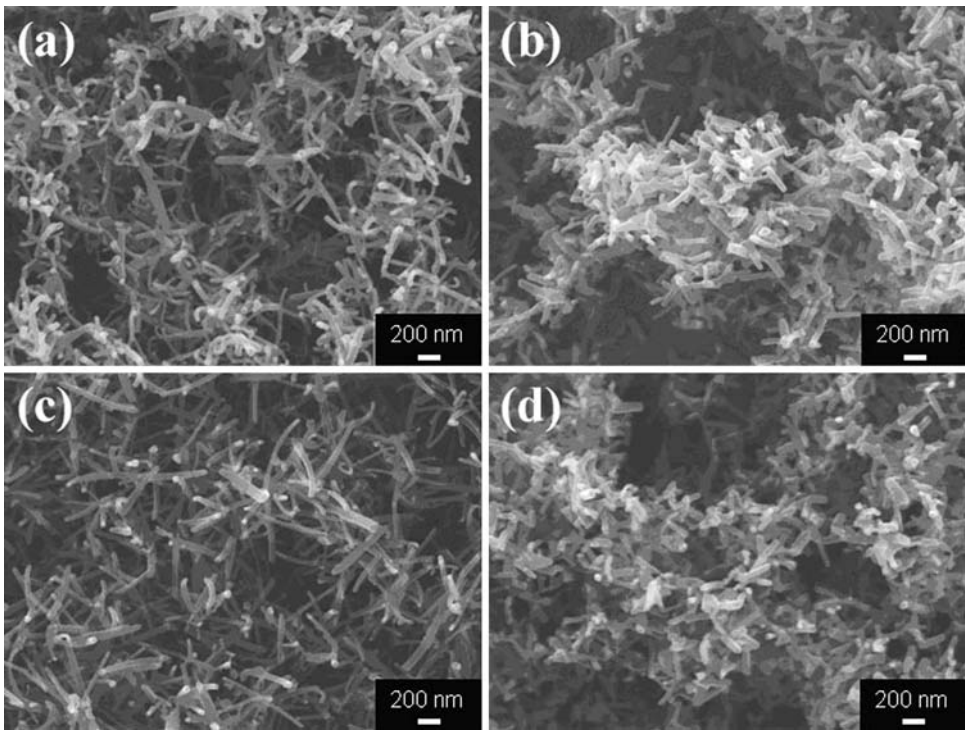

Fig. 1 FESEM micrographs of the Gaq_3 1D nanostructures fabricated in He of various working pressures at the working temperatures lower than 350 °C: **a** 10 torr at 310 °C, **b** 50 torr at 310 °C, **c** 10 torr at 330 °C, and **d** 50 torr at 330 °C

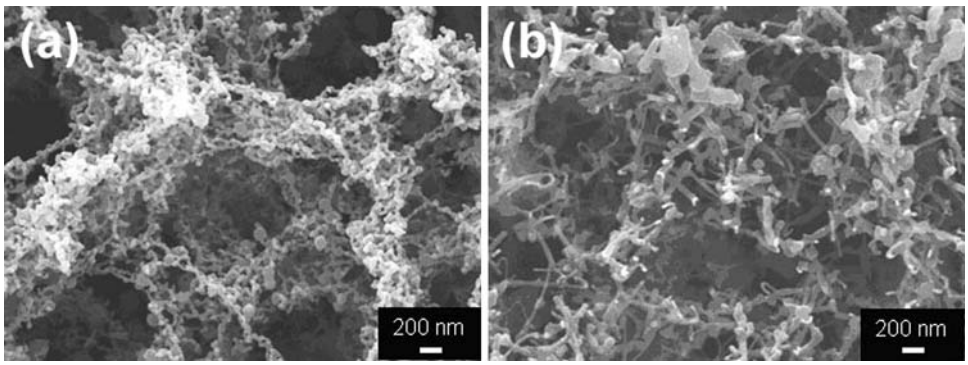

Fig. 2 FESEM micrographs of the Gaq_3 nanostructures fabricated at 370 °C in He of various working pressures: **a** 10 torr and **b** 50 torr

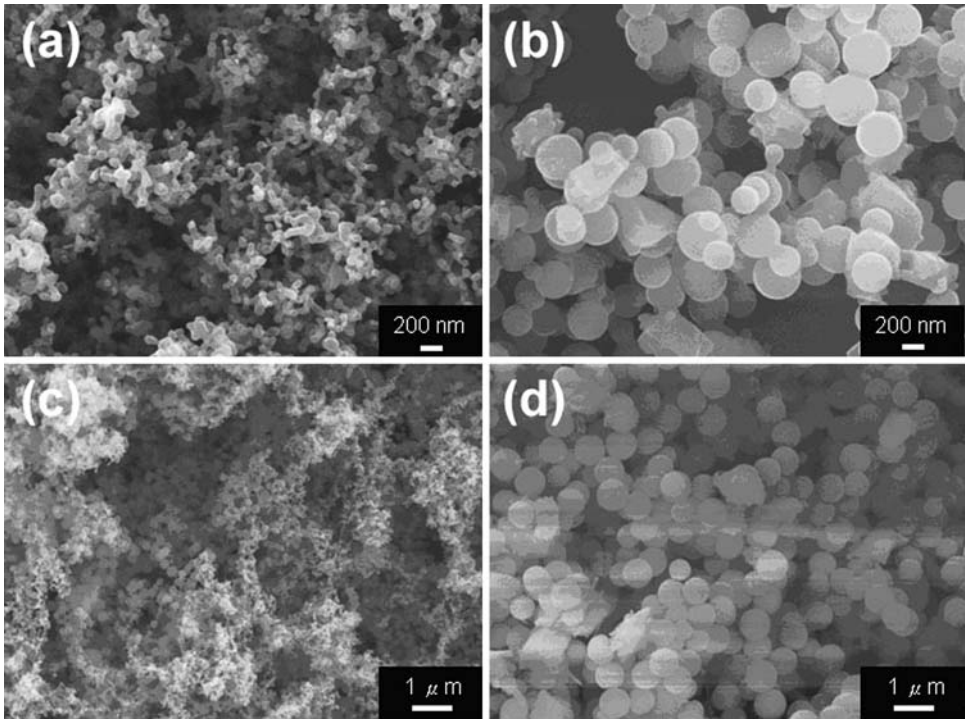

Fig. 3 FESEM micrographs of the Gaq_3 nanostructures fabricated in He of various working pressures at higher working temperatures: **a** 10 torr at 390 °C, **b** 50 torr at 390 °C, **c** 10 torr at 400 °C, and **d** 50 torr at 400 °C

(2) Working gas type

Similar results could also be observed when the working gas was changed to Ar under the same conditions of working pressures and temperatures (not shown). Since an Ar atom has a larger atomic size and weight than a He atom, the sublimed Gaq_3 molecules lose more energy after colliding with Ar atoms, and larger structures were thereby formed on the cold substrate. For example, as the working temperature is 390 °C and the working pressure is 50 torr, the average diameter of the nanospheres formed in He is, approximately, 300 nm (Fig. 3b), whereas that obtained in Ar is over 1 μm. Nevertheless, the sizes of He and Ar atoms are relatively small compared with a Gaq_3 molecule. Therefore, the type of working gas showed more negligible influences on the morphology and dimension of Gaq_3 nanostructures than working pressure and working temperature.

(3) Working temperature and working pressure

Unlike working gas, the working temperature for thermal evaporation affects the morphology and dimension of nanostructures significantly. When Gaq_3 molecules acquire enough thermal energy from the graphite boat heater, they are vaporized and sublime toward the substrate above. During the evaporation process, the sublimed molecules collide with the inert gaseous atoms within the chamber and thereby lose energy. As a result, small Gaq_3 nuclei form before they reach the substrate and are trapped on the cold substrate subsequently. More molecules adsorb onto the nuclei by intermolecular π–π interaction and the nuclei gradually grow into larger structures if the evaporation is continuously proceeding. At a lower working temperature, the flow rate of sublimed molecules is relatively lower and the nuclei are smaller, so there is more time for molecular adsorption and pileup along one-dimension to form 1-D

nanostructures. When a higher working temperature close to the melting point of Gaq_3 is applied, a large amount of sublimed molecules burst out in a short time and the flow rate of sublimed molecules is higher, so larger nuclei form before reaching the substrate, leading to the growth of larger spherical structures on the substrate. The formation of Gaq_3 nanowires at a lower working temperature and nanospheres at a higher working temperature was also demonstrated by Tian et al. [30] On the other hand, a higher working pressure for thermal evaporation causes higher collision frequency between sublimed molecules and inert gaseous atoms, resulting in nucleation and growth of larger structures as well. As revealed in Fig. 3a and b, the diameter of the nanospheres formed at 390 °C in He is around 60 nm as the working pressure is 10 torr, whereas that obtained at 50 torr increases and ranges from 200 to 400 nm. Consequently, it can be concluded that working pressure and working temperature are the two most crucial factors for the growth of Gaq_3 nanostructures.

(4) Structural characterization and spectroscopic analysis

The XRD patterns of Gaq_3 powder and the nanostructures fabricated at 350 and 400 °C in 10 torr of He are identified, as displayed in Fig. 4. Their crystallinity can be further confirmed by FTIR and NMR spectroscopy. According to the XRD data reported previously, the powder is mainly composed of β-phase Gaq_3. Both the 1-D nanostructures and nanospheres are mainly composed of δ-phase Gaq_3 [31, 32]. The similarity between crystalline Gaq_3 and Alq_3 can be revealed by comparing the XRD patterns of Gaq_3 nanostructures with those of α-phase and δ-phase Alq_3 [33]. Through FTIR analysis, it has been demonstrated that both α-phase and β-phase Gaq_3 consist

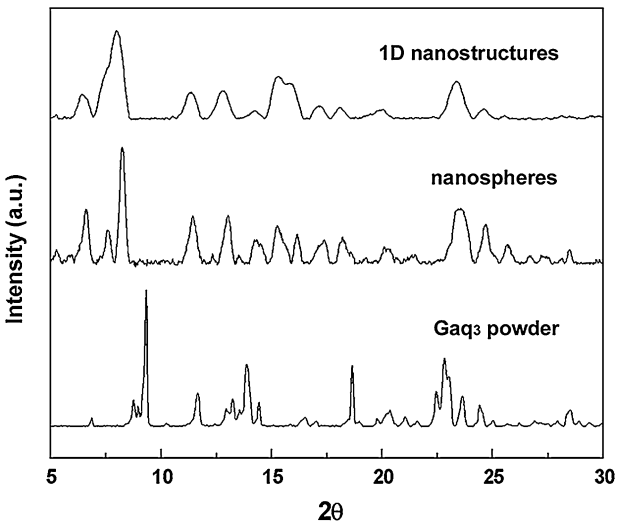

Fig. 4 XRD patterns of Gaq_3 powder and nanostructures. The 1-D nanostructures are obtained in 10 torr of He at 350 °C, and the nanospheres are formed in 10 torr of He at 400 °C

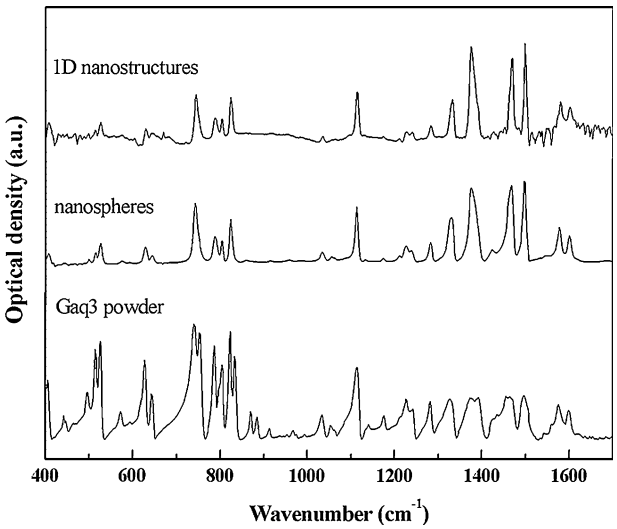

Fig. 5 FTIR spectra of Gaq_3 powder and nanostructures. The 1-D nanostructures are obtained in 10 torr of He at 330 °C, and the nanospheres are formed in 10 torr of He at 400 °C

of the meridional isomer and δ-phase Gaq_3 consists of the facial isomer [31]. In this work, the FTIR spectra of Gaq_3 powder and nanostructures are also measured, as displayed in Fig. 5. They show similar absorption peaks above 1,000 cm^{-1}. This is attributed to similar vibration modes of the hydroxyquinoline ligands no matter in the meridional form of Gaq_3 powder or the facial form of nanostructures. The principal fingerprints to discriminate the two isomers locate in the region of 720–850 cm^{-1} [31, 34]. In this region, the powder exhibits splitting peaks while the nanostructures show only single peaks without splittings. This again demonstrates the meridional form of Gaq_3 powder and the facial form of nanostructures. Although the absorption peaks below 600 cm^{-1} are contributed by the vibrations of metal–oxygen (M–O) and metal–nitrogen (M–N) bondings, the intensity is too weak to differentiate the two dissimilar isomeric states.

Unequivalent carbon atoms in a compound can be distinguish by ^{13}C NMR spectrum, as different electron densities arise from varied chemical environments. The isotropic resonance lines calculated by density functional theory (DFT) for the meridional and facial isomers of Alq_3 has been illustrated [35, 36]. The solution and solid-state ^{13}C NMR spectra of various Alq_3 crystalline phases has also been reported [37]. The solid-state ^{13}C NMR spectra demonstrated that both γ-phase and δ-phase Alq_3 consisted of the facial isomer and α-phase Alq_3 was composed of the meridional isomer. Moreover, Alq_3 existed as the meridional form in solutions [38]. Because the three ligands in the facial isomer were chemically equivalent, the electron density of the carbon atoms in each ligand was theoretically the same. Thus the DFT-calculated results revealed

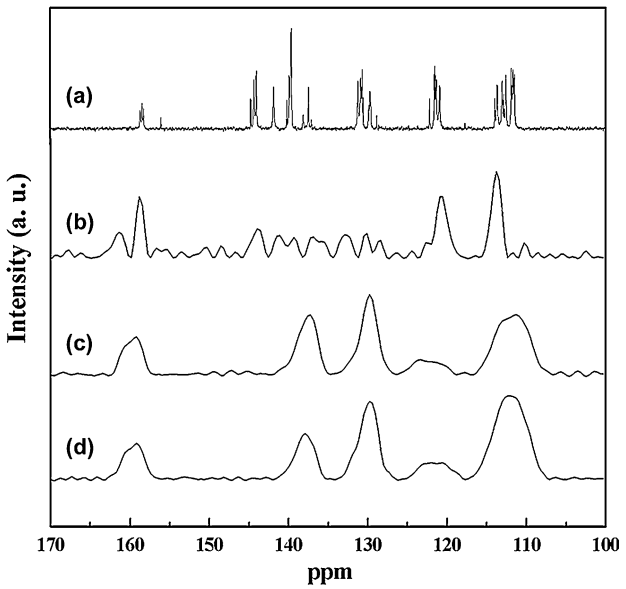

Fig. 6 Solution and solid-state ^{13}C NMR spectra of Gaq_3: (a) Gaq_3 dissolved in $CDCl_3$, (b) Gaq_3 powder, (c) 1D nanostructures formed in 10 torr of He at 350 °C, and (d) nanospheres obtained in 10 torr of He at 400 °C

only one single peak for each carbon atom. By contrast, the three ligands in the meridional isomer were chemically unequivalent, so the DFT-calculated peak of each carbon atom showed splittings. Based on above studies, similar analysis approaches were also applied to Gaq_3. The ^{13}C NMR spectra of Gaq_3 powder and nanostructures are displayed in Fig. 6. Because the characteristic chemical shifts of Gaq_3 in solutions approximates to those of Alq_3 in a solution state, it is deduced that Gaq_3 also exists as the meridional form in solutions (Fig. 6a). Although the resolution of the solid-state ^{13}C NMR spectra is inferior, it still can be noticed that the 1-D nanostructures and nanospheres exhibit similar spectra (Fig. 6c and d), while the spectrum of Gaq_3 powder is apparently different (Fig. 6b). It is then evidenced that the nanostructures consist of the facial isomer instead of the meridional isomer, i.e., they can be classified as δ-phase Gaq_3.

(5) Thermal analysis

The major difference between Gaq_3 and Alq_3 nanostructures is that Gaq_3 nanostructures are crystalline whereas Alq_3 nanostructures are amorphous [20–22]. Because the molecular weight of Alq_3 is lower than that of Gaq_3 and the working temperatures for evaporation of Alq_3 nanostructures are higher than those of Gaq_3 nanostructures; the energy loss and nucleation of sublimed Alq_3 molecules are rapid, resulting in faster growth of Alq_3 nanostructures on the substrate. The Alq_3 molecules can thereby stack in a more disordered way and generate the amorphous state. The formation of crystalline Gaq_3 nanostructures can be attributed to slower sublimation and growth so that Gaq_3 molecules are able to stack in a more ordered way. The thermal properties of Gaq_3 and Alq_3 nanostructures are also similar [20–22]. Both Gaq_3 and Alq_3 nanospheres exhibited two peaks on their DSC curves, implying two phase transitions occurred in their heating processes. One was at around 120–150 °C and the other was at around 350–390 °C. The one in the lower temperature region of amorphous Alq_3 nanospheres has been identified as a transition to α phase [20]. Since the melting point of Gaq_3 is around 10 °C lower than that of Alq_3, the intermolecular interaction of Gaq_3 is comparatively weaker. Thus, it is reasonable to deduce that the two-phase transition temperatures of Gaq_3 nanostructures are lower than those of Alq_3 nanostructures.

Figure 7 shows the DSC traces of Gaq_3 powder and the nanospheres formed in 30 torr of He at 400 °C. It reveals that the powder exhibits a large melting endothermic peak at 409.5 °C. Since the powder has been identified as β-phase Gaq_3 based on XRD, FTIR, and NMR analyses, the coupling peak including an endotherm at 385.8 °C and an adjacent exotherm at 389 °C can be ascribed to the phase transition from β to δ phase [16, 31]. This is a meridional to facial isomerization involving a ligand flip in the solid state. Besides the large melting endotherm at 403.7 °C, the nanospheres show another two small exothermic peaks at around 137 and 364 °C, respectively. The exotherm at 364 °C can also be ascribed to the phase transition of β to δ phase, lower than the transition temperature of Gaq_3 powder. With a large surface-to-volume ratio (specific area), the nanospheres exhibit higher surface energy and require less enthalpy for phase transition, leading to reduced temperatures of phase and melting transitions. It is then deduced that another small exotherm

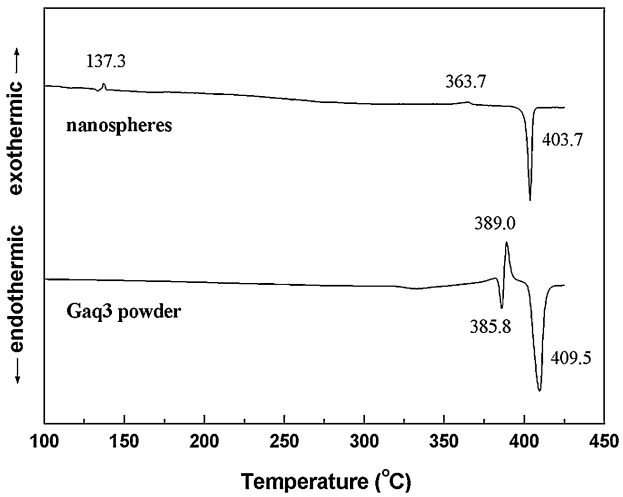

Fig. 7 DSC traces of Gaq_3 powder and the nanospheres fabricated in 30 torr of He at 400 °C

of the nanospheres at 137 °C is caused by the phase transition from δ to β phase. As the nanospheres were heated from room temperature to 137 °C, they gained enough energy to rearrange into a more stable low-temperature phase, and were subsequently transformed into δ phase at a higher temperature.

(6) Photoluminescence property

The PL spectra of Gaq_3 powder and nanostructures are examined, as shown in Fig. 8. The 1-D nanostructures and nanospheres are fabricated in 10 torr of He at 330 and 400 °C, respectively. All the spectra have a broad peak in the wavelength range of 400–700 nm. The emission maximum of Gaq_3 powder is at 518 nm. All the nanostructures show the same emission maximum at 508 nm regardless of their morphology and dimension. Thus, it is evident that the PL property of nanostructures is affected neither by morphology nor dimension, in accordance with previous studies [30, 39]. This indicates that Gaq_3 nanostructures present no quantum confinement effect due to the relatively weak van der Waals force among neighboring molecules [40]. Another worth mentioning phenomenon is that all the nanostructures exhibit a spectral blue shift of 10 nm. This can be interpreted by different isomeric states and intermolecular interactions between the nanostructures and Gaq_3 powder [37]. The molecular packing in the δ-phase nanostructures (facial form) has a looser interligand spacing compared to the β-phase powder (meridional form), consequently resulting in reduced orbital overlap and a spectral blue shift.

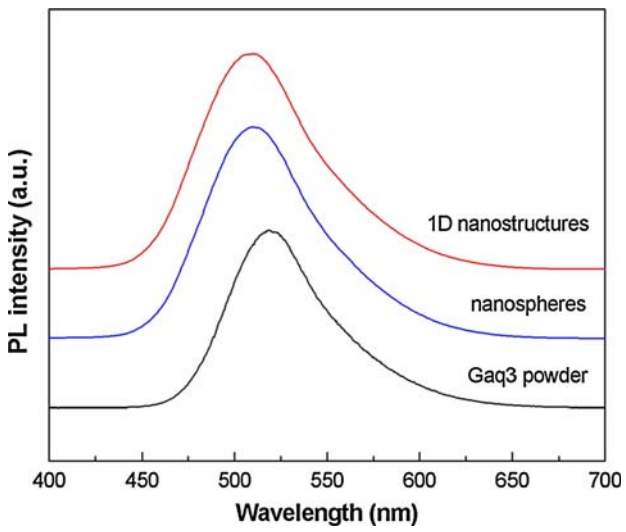

Fig. 8 PL spectra of Gaq_3 powder and nanostructures. The 1-D nanostructures are obtained in 10 torr of He at 330 °C, and the nanospheres are formed in 10 torr of He at 400 °C

Conclusions

This study has disclosed a physical thermal evaporation approach for fabrication of crystalline Gaq_3 nanospheres and 1-D nanostructures under cold trap. The influences of working gas, working temperature, and working pressure on the formation of the nanostructures were explored as well. It was demonstrated that their morphology and dimension were mainly controlled by working temperature and could be modulated by varying working pressure. A lower working temperature caused growth of 1-D nanostructures, whereas a higher working temperature resulted in formation of nanospheres. When working pressure increased, larger nanospheres were obtained. To summarize, 1-D crystalline nanostructures could be fabricated in He gas at 310–330 °C, and crystalline nanospheres could be formed in He gas at 390–400 °C. According to XRD, FTIR and NMR analyses, Gaq_3 raw powder was identified as β phase and the crystalline nanostructures mainly consisted of δ-phase Gaq_3. The DSC trace of crystalline nanospheres revealed two small exotherms in addition to the large melting endotherm, implying two phase transitions occurred during the heating process. The one in lower temperature region was ascribed to a transition from δ to β phase, and another in higher temperature region could represent a transition from β to δ phase. Due to absence of quantum confinement effect, all crystalline nanostructures show similar PL spectra with an emission maximum at around 508 nm regardless of their morphology and dimension. Compared with the β-phase powder, the δ-phase nanostructures had a loose molecular packing and interligand spacing, leading to decreased orbital overlap and a spectral blue shift.

Acknowledgment This work was supported by the National Science Council of Taiwan under Contract No. NSC 93-2216-E-007-034 and NSC 94-2216-E-007-029.

References

1. A.P. Alivisatos, P.F. Barbara, A.W. Castleman, J. Chang, D.A. Dixon, M.L. Klein, G.L. McLendon, J.S. Miller, M.A. Ratner, P.J. Rossky, S.I. Stupp, M.E. Thompson, Adv. Mater. **10**, 1297 (1999)
2. A. Thiaville, J. Miltat, Science **284**, 1939 (1999)
3. G.A. Ozin, Adv. Mater. **4**, 612 (1992)
4. C. Yan, J. Liu, F. Liu, J. Wu, K. Gao, D. Xue, Nanoscale Res. Lett. **3**, 473 (2008)
5. Y. Xia, P. Yang, Y. Sun, Y. Wu, B. Mayers, B. Gates, Y. Yin, F. Kim, H. Yan, Adv. Mater. **15**, 353 (2003)
6. W.U. Huynh, J.J. Dittmer, A.P. Alivisatos, Science **295**, 2425 (2002)
7. S. Iijima, Nature **351**, 56 (1991)
8. Z.W. Pan, Z.R. Dai, Z.L. Wang, Science **291**, 1947 (2001)
9. Y. Cao, I.D. Parker, G. Yu, C. Zhang, A.J. Heeger, Nature **397**, 414 (1999)

10. A. Noy, A.E. Miller, J.E. Klare, B.L. Weeks, B.W. Woods, J.J. De Yoreo, Nano Lett. **2**, 109 (2002)
11. J.H. Lim, C.A. Mirkin, Adv. Mater. **14**, 1474 (2002)
12. K.A. Sablon, Nanoscale Res. Lett. **3**, 395 (2008)
13. Q. Tang, Y. Tong, H. Li, Z. Ji, L. Li, W. Hu, Y. Liu, D. Zhu, Adv. Mater. **20**, 1511 (2008)
14. Q. Tang, H. Li, Y. Song, W. Xu, W. Hu, L. Jiang, Y. Liu, X. Wang, D. Zhu, Adv. Mater. **18**, 3010 (2006)
15. C.W. Tang, S.A. Van Slyke, Appl. Phys. Lett. **51**, 913 (1987)
16. L.S. Sapochak, A. Padmaperuma, N. Washton, F. Endrino, G.T. Schmett, J. Marshall, D. Fogarty, P.E. Burrows, S.R. Forrest, J. Am. Chem. Soc. **123**, 6300 (2001)
17. M. Ghedini, M.L. Deda, I. Aiello, A. Grisolia, Syn. Met. **138**, 189 (2003)
18. C.H. Chen, S. Shi, Coord. Chem. Rev. **171**, 161 (1998)
19. P.E. Burrows, Z. Shen, V. Bulovic, D.M. McCarty, S.R. Forrest, J. Appl. Phys. **79**, 7991 (1996)
20. C.P. Cho, C.A. Wu, T.P. Perng, Adv. Funct. Mater. **16**, 819 (2006)
21. C.P. Cho, T.P. Perng, Nanotechnology **17**, 3756 (2006)
22. C.P. Cho, T.P. Perng, Nanotechnology **18**, 125202 (2007)
23. J.J. Chiu, W.S. Wang, C.C. Kei, C.P. Cho, T.P. Perng, P.K. Wei, S.Y. Chiu, Appl. Phys. Lett. **83**, 4607 (2003)
24. M. Benyoucef, A. Rastelli, O.G. Schmidt, S.M. Ulrich, P. Michler, Nanoscale Res. Lett. **1**, 172 (2006)
25. D. Jiang, L. Cao, W. Liu, G. Su, H. Qu, Y. Sun, B. Dong, Nanoscale Res. Lett. **4**, 78 (2009)
26. P.E. Burrows, L.S. Sapochak, D.M. McCarty, S.R. Forrest, M.E. Thompson, Appl. Phys. Lett. **64**, 2718 (1994)
27. L.S. Sapochak, P.E. Burrows, D. Garbuzov, D.M. Ho, S.R. Forrest, M.E. Thompson, J. Phys. Chem. **100**, 17766 (1996)
28. A. Elschner, H.W. Heuer, F. Jonas, S. Kirchmeyer, R. Wehrmann, K. Wussow, Adv. Mater. **13**, 1811 (2001)
29. J.J. Chiu, W.S. Wang, C.C. Kei, T.P. Perng, Appl. Phys. Lett. **83**, 347 (2003)
30. X. Tian, J. Fei, Z. Pi, C. Yang, D. Luo, F. Pei, L. Zhang, Sol. Stat. Commun. **138**, 530 (2006)
31. M. Brinkmann, B. Fite, S. Pratontep, C. Chaumont, Chem. Mater. **16**, 4627 (2004)
32. M. Brinkmann, G. Gadret, M. Muccini, C. Taliani, N. Masciocchi, A. Sironi, J. Am. Chem. Soc. **122**, 5147 (2000)
33. M. Braun, J. Gmeiner, M. Tzolov, M. Coelle, F.D. Meyer, W. Milius, H. Hillebrecht, O. Wendland, J.U. Schütz, W. Brütting, J. Chem. Phys. **114**, 9625 (2001)
34. A.D. Esposti, M. Brinkmann, G. Ruani, J. Chem. Phys. **116**, 798 (2002)
35. M. Amati, F. Lelj, Chem. Phys. Lett. **358**, 144 (2002)
36. M. Amati, F. Lelj, J. Phys. Chem. A **107**, 2560 (2003)
37. H. Kaji, Y. Kusaka, G. Onoyama, F. Horii, J. Am. Chem. Soc. **128**, 4292 (2006)
38. M. Utz, C. Chen, M. Morton, F. Papadimitrakopoulos, J. Am. Chem. Soc. **125**, 1371 (2003)
39. C.H. Cheung, A.B. Djurisic, Y.H. Leung, Z.F. Wei, S.J. Xu, W.K. Chan, Chem. Phys. Lett. **394**, 203 (2004)
40. A.P. Alivisatos, Science **271**, 933 (1996)